Monte Carlo studies of the dynamical response of quantum many-body systems

H. -B. Schüttler and D. J. Scalapino
Department of Physics, University of California, Santa Barbara, California 93106
(Received 15 October 1985)

We present a method to obtain dynamical correlation functions of quantum many-body systems in the real-frequency domain from Monte Carlo data of the corresponding imaginary-time Green's functions. The method is based on a least-squares-fit procedure to solve the integral equation relating imaginary-time and real-frequency correlation functions. To demonstrate its feasibility, we have applied our method to imaginary-time Monte Carlo data for the density correlation function of a simple model of interacting spinless fermions in one dimension. We compare our results to the analytical results, available in the limits of zero and strong interaction. We find that despite the presence of noise in the input data, the real-frequency spectra obtained with our method are qualitatively correct. They reflect accurately the particle-hole and the soliton-antisoliton excitations, present in the noninteracting and in the strongly coupled fermion system, respectively. We also compare our method to other approaches that have been proposed for obtaining dynamical correlation functions via Monte Carlo simulation.

I. INTRODUCTION

In recent years, Monte Carlo (MC) methods have become a powerful tool for the investigation of the thermodynamics and static correlations of quantum many-body systems.[1] However, little progress has been made so far in the development of MC techniques that would allow the study of the real-time dynamics of such systems. Recent attempts to directly simulate real-frequency[2] or real-time[3] correlation functions have dealt only with the simplest (one degree-of-freedom) model systems and have given reasonable results only after an exceedingly large number of MC steps. Also, Padé approximants have been used to analytically continue imaginary-time MC data for single degree-of-freedom models.[4] Considering the enormous amounts of computation time required, it seems difficult to apply these methods to many-particle systems.

Recently, we have proposed a procedure to extract real-frequency self-correlation functions from the corresponding imaginary-time Green's functions of many-particle systems that can be simulated by standard quantum MC techniques.[5] Here, we present a more detailed account of this method. We should emphasize from the outset that, given a finite set of "noisy" MC data for the imaginary-time Green's function, one should expect, at best, qualitatively correct results for the corresponding real-frequency spectral function. Roughly speaking, one encounters the difficulty that the imaginary-time Green's function is very insensitive to the structure of the underlying spectral function. Hence, even small statistical errors in the MC input data can give rise to large errors in the resulting spectral function. It is the purpose of the present paper to explore possibilities of extracting the maximum amount of information about the spectral function that is contained in such noisy input data.

In Sec. II, we will summarize the general properties of the various types of real-time correlation functions that are of physical interest. We also derive the basic integral equation which expresses the imaginary-time Green's functions in terms of a real-frequency spectral function.

In Sec. III, we discuss the difficulties of solving this integral equation (to obtain the spectral function) in the presence of noise in the imaginary-time input data. We then outline a method to achieve such a solution. The crucial ingredient of our procedure is to include as a constraint on the solution the fact that the real-frequency spectrum of a self-correlation function is positive. In addition, we take into account not only MC data of the imaginary-time Green's function itself, but also independently simulated data for its first and second derivatives.

To demonstrate the feasibility of our approach, we have applied it to a simple one-dimensional (1D) model of spinless fermions.[6,7] In Sec. IV, we discuss the results obtained for the density correlation function of this system and compare them to exact and approximate analytical results, valid in the limits of a noninteracting and a strongly coupled system, respectively. For the noninteracting case, we demonstrate that the results of our procedure are qualitatively in agreement with the exact results and stable against noise and changes of various "arbitrary" parameters. We also discuss and compare our procedure to other methods that might be used to extract real-frequency spectra from imaginary-time data. For the strongly coupled system, we discuss the dynamics of soliton creation and diffusion as reflected in the spectrum of the density correlation function. We show that the essential features of the spectrum are accurately reproduced in our results obtained from MC data.

Section V contains a brief summary of the results and concluding remarks.

II. DYNAMICAL CORRELATION FUNCTIONS

Let us briefly summarize a few general properties of the various types of time-dependent correlation functions that will be of interest to us in the following. For the time be-

ing, we want to assume only that the physical system is described by some (Hermitian) Hamiltonian operator H. We consider the time-dependent correlations between two arbitrary operators, A and B, which need not be Hermitian, unless it is specified explicitly.

Quantum Monte Carlo methods allow us to obtain the imaginary-time Green's function, defined as

$$G_{AB}(\tau)=\langle A(-i\tau)B\rangle \equiv \frac{1}{Z}\mathrm{tr}[e^{-\beta H}A(-i\tau)B] , \tag{2.1}$$

where

$$A(t)=e^{itH}Ae^{-itH} . \tag{2.2}$$

$Z=\exp(-\beta H)$ is the partition function at temperature $k_BT=1/\beta$, and τ is limited to $0\le\tau\le\beta$.

On the other hand, the experimentally observable linear response of the system is given in terms of real-time correlation functions of the form

$$S_{AB}(t)\equiv\langle A(t)B\rangle \tag{2.3}$$

and

$$\chi_{AB}(t)\equiv i\langle[A(t),B]_-\rangle , \tag{2.4}$$

where $[\,,\,]_-$ denotes the commutator. For example, the dynamical structure factor can be written as the time Fourier transform of some $S_{AB}(t)$,

$$S_{AB}(\omega)=\int_{-\infty}^{\infty}dt\,e^{i\omega t}S_{AB}(t) . \tag{2.5}$$

Quantities like the frequency-dependent conductivity are given by the retarded ($z=\omega+i0^+$) part of the two-sided Laplace transform of some $\chi_{AB}(t)$,

$$\chi_{AB}(z)=\sigma\int_{-\infty}^{\infty}dt\,\Theta(\sigma t)e^{izt}\chi_{AB}(t) , \tag{2.6}$$

where z is a complex frequency with $\mathrm{Im}z\neq0$, $\sigma=\mathrm{sgn}(\mathrm{Im}z)$, and $\Theta(\sigma t)$ denotes the step function.

For our purposes, it is convenient to introduce the correlation function,

$$\phi_{AB}(t)=i\langle[A(t),B]_+\rangle \tag{2.7}$$

[and, analogous to (2.8), its two-sided Laplace transform $\phi_{AB}(z)$] where in (2.7), $[\,,\,]_+$ denotes the anticommutator. Although ϕ_{AB} itself is not of physical interest, it is directly related to the physically relevant linear-response functions S_{AB} and χ_{AB}. On the other hand, $\phi_{AB}(z)$ is in a simple way connected with G_{AB}. These relationships are conveniently formulated in terms of the spectral functions defined at real frequencies ω by

$$\phi''_{AB}(\omega)=\frac{1}{2i}[\chi_{AB}(z=\omega+i0^+)-\chi_{AB}(z=\omega-i0^+)] =\frac{1}{2i}\int_{-\infty}^{\infty}dt\,e^{i\omega t}\chi_{AB}(t) , \tag{2.8}$$

and, analogously, $\chi''_{AB}(\omega)$. They contain the complete information about the full complex frequency functions, $\phi_{AB}(z)$ and $\chi_{AB}(z)$, respectively, since, for example,

$$\phi_{AB}(z)=\int\frac{d\omega}{\pi}\frac{\phi''_{AB}(\omega)}{\omega-z} . \tag{2.9}$$

The connection between S_{AB}, χ_{AB}, and ϕ_{AB} is summarized by

$$S_{AB}(\omega)=2\phi''_{AB}(\omega)/(1+e^{-\beta\omega}) , \tag{2.10}$$

$$\chi''_{AB}=\phi''_{AB}(\omega)\tanh\frac{\beta\omega}{2} . \tag{2.11}$$

Hence, the physically relevant correlation functions, $\chi_{AB}(z)$ and $S_{AB}(\omega)$, can be easily constructed from $\phi''_{AB}(\omega)$.

On the other hand, $G_{AB}(\tau)$ is given in terms of $\phi_{AB}(z)$ by

$$G_{AB}(\tau)=\frac{1}{\beta}\sum_{i\omega_n}e^{-i\omega_n\tau}\phi_{AB}(z=i\omega_n),\quad 0\le\tau\le\beta \tag{2.12}$$

[where $\omega_n=\pi(2n+1)/\beta$, $n=0,\pm1,\pm2,\ldots$] and hence in terms of $\phi''_{AB}(\omega)$, by

$$G_{AB}(\tau)=\int_{-\infty}^{\infty}\frac{d\omega}{\pi}\frac{1}{1+e^{-\beta\omega}}e^{-\tau\omega}\phi''_{AB}(\omega) . \tag{2.13}$$

The problem of converting the imaginary-time Green's function into the real-frequency correlation function is thus reduced to solving this integral equation (2.13).

Of particular interest in the following is the case of self-correlation functions, that is, $B=A^\dagger$, where $\phi''_{AA^\dagger}(\omega)$ is real valued and positive in the sense that

$$\phi''_{AA^\dagger}(\omega)\ge0 . \tag{2.14}$$

If the operators A and B are Hermitian, i.e., $A=A^\dagger$, $B=B^\dagger$, $\phi_{AB}(t)$ [as defined in (2.7)] is purely imaginary, and the self-correlation function satisfies

$$\phi''_{AA}(\omega)=\phi''_{AA}(-\omega)\ge0 . \tag{2.15}$$

Finally, we should point out the connection between the imaginary-time Green's function $G_{AB}(\tau)$ and the sum rules obeyed by $S_{AB}(\omega)$, $\chi''_{AB}(\omega)$, and $\phi''_{AB}(\omega)$, namely,

$$G^{(m)}_{AB}(\tau)\Big|_{\tau=0}=\int_{-\infty}^{\infty}\frac{d\omega}{2\pi}(-\omega)^mS_{AB}(\omega) , \tag{2.16}$$

where $m=0,1,2,\ldots$ and $G^{(m)}_{AB}(\tau)$ denotes the mth derivative. Furthermore, if $\phi''_{AB}(\omega)=\phi''_{AB}(-\omega)$ [e.g., for the self-correlation function of a Hermitian operator $A=B=A^\dagger$, Eq. (2.15)], we have

$$G^{(m)}_{AB}(\tau)\Big|_{\tau=0}=\int_{-\infty}^{\infty}\frac{d\omega}{\pi}(-\omega)^m\phi''_{AB}(\omega) , \quad m=0,2,4,\ldots , \tag{2.17}$$

$$G^{(m)}_{AB}(\tau)\Big|_{\tau=0}=\int_{-\infty}^{\infty}\frac{d\omega}{\pi}(-\omega)^m\chi''_{AB}(\omega) , \quad m=1,3,5,\ldots . \tag{2.18}$$

Hence, $G^{(m)}_{AB}(\tau=0)$ contains the mth moment of $S_{AB}(\omega)$ and also the mth moment of $\phi''_{AA}(\omega)$ and $\chi''_{AA}(\omega)$ in the case $A=B=A^\dagger$.

III. CONVERSION FROM IMAGINARY TIME TO REAL FREQUENCY

A. Overview

As pointed out in Sec. II, the spectral function $\phi''_{AB}(\omega)$ can be obtained from $G_{AB}(\tau)$ as the solution of the integral equation (2.13). This would be a straightforward numerical exercise if $G_{AB}(\tau)$ were given with arbitrary accuracy for an arbitrarily large number of τ values. We could, for example, start from some approximate trial function ϕ_F,

$$\phi''_{AB}(\omega)\cong\phi_F(\omega;a_1,\ldots,a_F)\equiv\sum_{l=1}^{F}a_l\phi_l(\omega)\ , \tag{3.1}$$

where $\phi_l(\omega)$ is an appropriately chosen complete set of orthogonal (or at least linearly independent) functions. We would then vary the amplitudes a_l so as to minimize the "mean squared deviation" function [not to be confused with $S(\omega)$, Eq. (2.5)]

$$S(a_1,\ldots,a_F)\equiv\int_0^\beta d\tau\left[G_{AB}(\tau)-\int_{-\infty}^{\infty}\frac{d\omega}{2\pi}K(\tau,\omega)\phi_F(\omega;a_1,\ldots,a_F)\right]^2\ , \tag{3.2}$$

where

$$K(\tau,\omega)\equiv 2e^{-\tau\omega}/(1+e^{-\beta\omega})\ . \tag{3.3}$$

By taking

$$0=\frac{\partial S}{\partial a_l},\quad l=1,\ldots,F\ , \tag{3.4}$$

a set of F linear equations for $a_1,\ldots,a_F$ results which is readily solved numerically. With a sufficiently large number, F, of "fit" parameters a_l, we should then obtain $\phi''_{AB}(\omega)$ with (in principle) arbitrary accuracy.

In a Monte Carlo calculation, however, $G_{AB}(\tau)$ is calculated at only a limited number of τ_i values ($i=0,\ldots,L$). We can still follow the "least-squares" approach, outlined above, if we replace the τ integral in (3.2) by a sum over the discrete τ_i values. However, we then have to restrict the number of fit parameters to

$$F\leq L \tag{3.5}$$

[otherwise the set of linear equations (3.4) becomes singular and the solutions are no longer unique]. It is clear that this in turn limits the "resolution" of our "measurement" of $\phi''_{AB}(\omega)$.

Even more severe limitations, however, arise from the fact that all MC data are "noisy:" Roughly speaking, the difficulty is that a small statistical error in the input data, $G_{AB}(\tau_i)$, will in general lead to a large error in the spectral function $\phi''_{AB}(\omega)$, when the simple linear conversion procedure [Eqs. (3.1)–(3.4)] is applied. To understand this, it is instructive to consider the behavior of the integral kernel, $K(\tau,\omega)$, shown in Fig. 1(a) as a function of ω for various values of τ: For $0<\tau<\beta/2$, it exhibits a broad peak at positive frequencies with a width of the order $1/\tau$. In the limit $|\omega|\gg\tau^{-1},(\beta-\tau)^{-1}$, it falls off like $\exp[-\tau(\omega)]$ for $\omega>0$ and like $\exp[(\beta-\tau)\omega]$ for $\omega<0$. When τ reaches $\beta/2$, the peak is centered around $\omega<0$, and for $\beta/2<\tau<\beta$ it appears at negative frequencies, since

$$K(\tau,-\omega)=K(\beta-\tau,\omega)\ . \tag{3.6}$$

Clearly, $K(\tau,\omega)$ is a quite structureless object, and the imaginary-time Green's function $G_{AB}(\tau)$, obtained by integrating over $\phi''_{AB}(\omega)$ with $K(\tau,\omega)$ as a "weight" function, is insensitive to the detailed behavior of ϕ''_{AB}.

Notice, however, that the (first and second) τ derivatives,

$$\left[\frac{\partial}{\partial\tau}\right]^m K(\tau,m)=(-\omega)^m K(\tau,m)\ , \tag{3.7}$$

displayed in Figs. 1(b) and 1(c), show a different peak structure than $K(\tau,\omega)$ itself. The τ derivatives of $G_{AB}(\tau)$,

$$G^{(m)}_{AB}(\tau)=\int\frac{d\omega}{2\pi}K(\tau,\omega)(-\omega)^m\phi''_{AB}(\omega)\ , \tag{3.8}$$

contain the same spectral function $\phi''_{AB}(\omega)$ under the integral, weighted, however, with $K(\tau,\omega)(-\omega)^m$ instead of just $K(\tau,\omega)$. One would, therefore, expect that the derivatives, when measured independently with the same accuracy as $G_{AB}(\tau)$, should reveal more detailed information

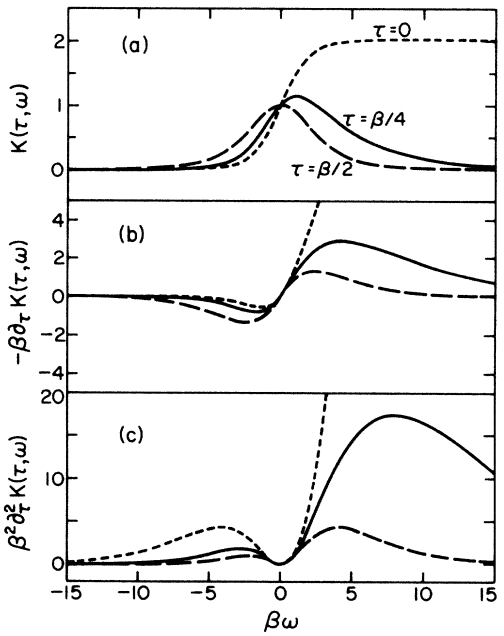

FIG. 1. Integral kernal $K(\tau,\omega)$ and τ derivatives for $\tau=0$ (· · · ·), $\beta/4$ (——), and $\beta/2$ (— — —).

about the underlying spectral function $\phi''_{AB}(\omega)$, at least, for frequencies ω larger than the thermal frequency $1/\beta$.

B. Conversion procedure

After these preliminary remarks, let us now describe our conversion method.

First of all, we restrict ourselves to self-correlation functions $G_{AA^\dagger}(\tau)$ for which $\phi''_{AA^\dagger}(\omega)$ is positive, as pointed out in the preceding section [Eq. (2.25)]. This property turns out to be a very important piece of information, and our method relies heavily on it.

Using Monte Carlo techniques, we "measure" $G(\tau)$ and, independently, the first few (two, in the sample calculations discussed in Sec. IV) of its τ derivatives, using the relationships

$$\frac{d}{d\tau}G(\tau)=\langle[H,A(-i\tau)]_-A^\dagger\rangle\ ,$$
$$\left[\frac{d}{d\tau}\right]^2 G(\tau)=\langle[H,[H,A(-i\tau)]_-]_-A^\dagger\rangle\ , \tag{3.9}$$

and so on. (For notational convenience, the subscripts $AA^\dagger$ are omitted here and in the following.)

To extract information about the spectral function from these data, we employ, basically, a least-squares-fit procedure, similar to the one outlined above: We introduce a trial function $\phi_F(\omega;a_1,\ldots,a_F)$ of the form (3.1) with basis functions ϕ_l (yet to be specified), and a "sum-of-squares" function

$$S(a_1,\ldots,a_F)=\frac{1}{N_{\rm MC}}\sum_i\sum_m\{[G^{(m)}_{\rm MC}(\tau_i)-G^{(m)}_F(\tau_i;a_1,\ldots,a_F)]/\Delta G^{(m)}_{\rm MC}(\tau_i)\}^2\ . \tag{3.10}$$

In (3.10), $G^{(m)}_{\rm MC}(\tau_i)$ denotes the MC data for the mth derivative ($m=0,1,2,\ldots$) of $G(\tau)$,

$$G^{(m)}_F(\tau_i;a_1,\ldots,a_F)=\int_{-\infty}^{\infty}\frac{d\omega}{2\pi}K(\tau_i,\omega)(-\omega)^m\phi_F(\omega;a_1,\ldots,a_F) \tag{3.11}$$

the corresponding fit. $\Delta G^{(m)}_{\rm MC}(\tau_i)$ is the standard deviation of $G^{(m)}_{\rm MC}(\tau_i)$, and $N_{\rm MC}$ is the total number of data points $G^{(m)}_{\rm MC}(\tau_i)$ included in S. We then minimize S with respect to the amplitudes a_l. However, we do not permit arbitrary values of $a_1,\ldots,a_F$ but rather impose the *constraint* that only those values are allowed in minimizing S for which

$$\phi_F(\omega;a_1,\ldots,a_F)\geq 0 \tag{3.12}$$

at all values of ω. We will demonstrate later on (Fig. 8) that this constraint is essential in stabilizing the fit result ϕ_F against large, unphysical statistical fluctuations.

To carry out the minimization, let us write S explicitly as a function of $a_1,\ldots,a_F$. By inserting (3.1) into (3.11), and then (3.11) into (3.10), we obtain

$$S=\sum_{l,l'=1}^{F}P_{ll'}a_la_{l'}+\sum_{l=1}^{F}X_la_l+S_0\ , \tag{3.13}$$

where

$$P_{ll'}=\sum_\mu g_\mu^2R_{\mu l}R_{\mu l'}\ , \tag{3.14}$$

$$X_l=\sum_\mu g_\mu^2G_\mu R_{\mu l}\ , \tag{3.15}$$

$$S_0=\sum_\mu g_\mu^2G_\mu^2\ , \tag{3.16}$$

$$G_\mu\equiv G^{(m)}_{\rm MC}(\tau_i),\quad \mu\equiv(m,i)\ , \tag{3.17}$$

$$g_\mu=[N_{\rm MC}^{1/2}\Delta G^{(m)}_{\rm MC}(\tau_i)]^{-1}\ , \tag{3.18}$$

$$R_{\mu l}=\int\frac{d\omega}{2\pi}K(\tau_i,\omega)(-\omega)^m\phi_l(\omega)\ . \tag{3.19}$$

Clearly, under the condition (3.12), the minimization of S becomes a nonlinear problem. However, it can be reduced to a series of linear equations (allowing a complete solution of the problem) by an appropriate choice of the basis functions $\phi_l(\omega)$ in (3.1). One such choice, the one that we will apply in the following, is a "histogram" representation, i.e., the ϕ_l are chosen to be nonoverlapping rectangular blocks of a certain width ΔW (to be specified later on).

$$\phi_l(\omega)=\begin{cases}1, & (l-1)\Delta W<\omega<l\Delta W\\ 0, & \text{otherwise}\ ,\end{cases} \tag{3.20}$$

for $l=1,2,\ldots,F$. If the spectral function $\phi''(\omega)$ is nonsymmetric [i.e., $\phi''(-\omega)\neq\phi''(\omega)$ for certain ω], we introduce an analogous set of blocks at negative frequencies. However, in many cases of interest, we know that

$$\phi''(\omega)\equiv\phi''(-\omega) \tag{3.21}$$

(for example, if A is Hermitian) and may hence choose a symmetric trial function right from the beginning. In this case, we take (3.20) as the definition of $\phi_l(\omega)$ for $\omega>0$ and define

$$\phi_l(\omega)=\phi_l(-\omega),\quad \omega<0\ , \tag{3.22}$$

i.e., $\phi_l(\omega)$ consists of two blocks of width ΔW, positioned symmetrically around $\omega=0$. A typical example of such a $\phi_F(\omega;a_1,\ldots,a_F)$ is shown in Fig. 2.

With this set of basis functions, the constraint (3.12) is equivalent to

$$a_l\geq 0,\quad l=1,\ldots,F\ . \tag{3.23}$$

It can easily be taken into account by setting

$$a_l=b_l^2,\quad l=1,\ldots,F \tag{3.24}$$

where the parameters b_l are arbitrary real numbers. To minimize S with respect to the b_l, we have to solve the system of nonlinear equations

$$0=\partial S(b_1^2,\ldots,b_F^2)/\partial b_l$$
$$=4\left[\sum_{l'} P_{ll'}b_{l'}^2-X_l\right]b_l,\quad l=1,\ldots,F\ . \tag{3.25}$$

From (3.25) it follows that, for a particular value of l, either b_l *or* the term within large parentheses (or both) vanishes. The complete set of (in general complex) solutions of (3.25) can therefore be obtained as follows. For a certain subset of l's, $l_1,\ldots,l_K$ ($K\le F$), say, we choose

$$b_{l_1}=\cdots=b_{l_K}=0\ . \tag{3.26}$$

For the other l's we solve a system of linear equations for b_l^2:

$$0=\sum_{\substack{l'=1\\ l'\neq l_1,\ldots,l_K}} P_{ll'}b_{l'}^2-X_l\ ,\quad l=1,\ldots,F;\ l\neq l_1,\ldots,l_K\ . \tag{3.27}$$

There are 2^F subsets $l_1,\ldots,l_K$ and hence (at most) 2^F solutions of (3.25). From those, we select the ones for which

$$b_l^2\ge 0,\quad l=1,\ldots,F\ , \tag{3.28}$$

and out of those, *the* one which gives the smallest value for $S(b_1^2,\ldots,b_F^2)$. This is the absolute minimum of $S(a_1,\ldots,a_F)$ under the constraint (3.12).

We should emphasize at this point that the above-described minimization procedure can be applied whenever the basis functions $\phi_l(\omega)$ are positive [in the sense of Eq. (2.14)] and "nonoverlapping" [in the sense that, for any two, l and l' ($l'\neq l$), $\phi_{l'}(\omega)$ vanishes wherever $\phi_l(\omega)$ does not].

A comment concerning our particular choice of basis functions ϕ_l is now in place: First of all, let us point out that it is flexible enough to approximate any positive function $\phi''(\omega)$ with arbitrary accuracy: We just have to allow for a large enough number of blocks with a small enough width ΔW. In *praxis*, however, this will hardly be the problem since, as we pointed out at the beginning, our "measurement" of $\phi''(\omega)$ is subject to a limited resolution, depending on the statistical quality and number of input data. The finite-block width ΔW takes this limited resolution into account.

This brings us to the question of how to choose ΔW. Obviously, the fit results, $a_1,\ldots,a_F$, and $S(a_1,\ldots,a_F)$ depend on ΔW or, equivalently, on the total width of the spectral function,

$$W=F\Delta W\ . \tag{3.29}$$

One possible approach to selecting a value for W is to use it as an additional fit parameter: Let us denote the (absolute) minimum value of $S(b_1^2,\ldots,b_F^2)$ for a given value of W and F by

$$S_F=S_F(W)\ . \tag{3.30}$$

For a typical set of MC data (the details of which will be described below) and for values of $F=2$, 3, and 4, we have displayed $S_F(W)$ in Fig. 5(a). It clearly exhibits local minima. For a given value of F, we select that value, $W_F^{(0)}$, for which $S_F(W)$ attains its absolute minimum. (The significance of the secondary local minima will be discussed in the following section.)

Notice that, as one would expect, $S_F[W_F^{(0)}]$ will saturate to some final absolute minimal value as we increase F further (Fig. 6). We then choose the smallest value of F for which $S_F(W_F)$ comes within, say, a few percent of this saturation value.

In this way, we have, finally, determined all the parameters that enter into our fit result ϕ_F. Our procedure of selecting F, the number of blocks, and $W=W_F$, the total width of the spectrum, may appear somewhat arbitrary. However, as we will discuss in the following section, the final result ϕ_F does not depend crucially on F and W (when varied within reasonable limits).

In concluding this section, we should point out that certain sum rules will automatically be satisfied by the real-frequency correlation functions obtained from our fit procedure. Namely, the correlation function $S(\omega)$ [obtained from the fit result for $\phi''(\omega)$ by multiplying with the thermal factor (2.10)] obeys the mth sum rule, (2.16) [to within the statistical accuracy of the MC value of $G^{(m)}(\tau=0)$] if $G^{(m)}(\tau=0)$ is included in the sum of squares (3.10). Furthermore, if $\phi''(-\omega)=\phi''(\omega)$, the fit result for $\phi''(\omega)$ and $\chi''(\omega)$ [obtained from the fit result for $\phi''(\omega)$ via (2.11)] will obey the mth sum rules, (2.17) and (2.18), respectively, if $G^{(m)}(\tau=0)$ is included in the fit.

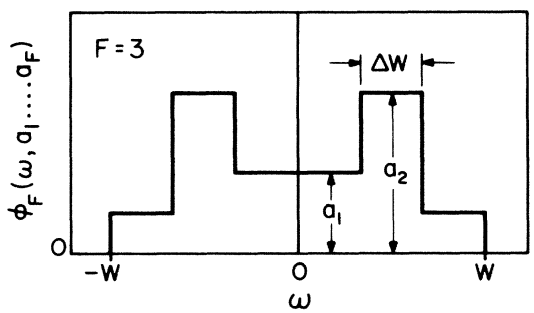

FIG. 2. Typical trial function $\phi_F(\omega;a_1,\ldots,a_F)$ for $F=3$.

IV. APPLICATION TO A SIMPLE MODEL: SPINLESS FERMIONS IN ONE DIMENSION

A. The model

To test our method, we apply it to a simple model, a 1D system of spinless fermions,[6] described by the Hamiltonian

$$H=\sum_{1\le j\le N}[-t(c_j^\dagger c_{j+1}+\text{H.c.})+Vn_jn_{j+1}]\ , \tag{4.1}$$

where c_j ($c_j^\dagger$) annihilates (creates) a fermion at lattice site j,

$$n_j=c_j^\dagger c_j \tag{4.2}$$

is the occupation number at that site, and N is the total number of sites in the chain. We restrict ourselves to even values of N.[8] Furthermore, we assume periodic boundary

conditions, i.e.,

$$c_{j\pm N}\equiv c_j \ , \tag{4.3}$$

for arbitrary j. In (4.1), the first term, involving the overlap integral t gives rise to single-particle transfer between nearest-neighbor sites. The second term describes an intersite repulsion (for $V>0$) between two particles.

Using the "world-line" MC algorithm,[8] we simulate the density correlation function

$$G(\tau,k)=\frac{1}{N}\sum_{1\le j,j'\le N} e^{-ik(j-j')}[\langle n_j(-i\tau)n_{j'}(0)\rangle - \langle n_j\rangle\langle n_{j'}\rangle]$$

$$=\langle \tilde{n}_k(-i\tau)\tilde{n}_k^{\dagger}(0)\rangle \ , \tag{4.4}$$

where

$$\tilde{n}_k=N^{-1/2}\sum_{1\le j\le N} e^{-ikj}(n_j-\langle n_j\rangle) \ , \tag{4.5}$$

$$k=\frac{2\pi}{N}\eta, \quad \eta=-\frac{N}{2}+1,\ldots,\frac{N}{2}-1,\frac{N}{2} \ . \tag{4.6}$$

Here $\langle\ \rangle$ denotes the thermal average in the canonical ensemble, i.e., the total number of fermions

$$N_F\equiv\sum_j n_j \tag{4.7}$$

is fixed.

Since the Hamiltonian (4.1) is invariant under translations ($j\to j+l$) and spatial inversion ($j\to N-j$), we have

$$\langle \tilde{n}_k(t)\tilde{n}^{\dagger}_{k'}(0)\rangle=0, \quad k\neq k' \tag{4.8}$$

and

$$\langle n_k^s(t)n_{k'}^c(0)\rangle=0 \quad (\text{all } k,k') \ , \tag{4.9}$$

where

$$n_k^s\equiv(2/N)^{1/2}\sum_k \sin(kj)(n_j-\langle n_j\rangle) \ , \tag{4.10}$$

$$n_k^c\equiv(2/N)^{1/2}\sum_k \cos(kj)(n_j-\langle n_j\rangle) \ . \tag{4.11}$$

It is then easily shown that the self-correlation function of

$$\tilde{n}_k=2^{-1/2}(n_k^c+in_k^s)=\tilde{n}^{\dagger}_{-k} \tag{4.12}$$

is in fact identical with that of n_k^s: In terms of the ϕ-correlation function, for example, we have

$$\phi(t,k)\equiv i\langle[\tilde{n}_k(t),\tilde{n}^{\dagger}_k(0)]_+\rangle = i\langle[n_k^s(t),n_k^s(0)]_+\rangle \ . \tag{4.13}$$

Hence, using (2.15), its spectral function satisfies

$$\phi''(\omega,k)=\phi''(-\omega,k)=\phi''(-\omega,k) \ , \tag{4.14}$$

since n_k^s is Hermitian. Furthermore [from Eq. (2.13)],

$$G(\tau,k)=G(\beta-\tau,k)=G(\beta-\tau,-k) \ . \tag{4.15}$$

Therefore, we have to consider only positive wave vectors, $k>0$. [Note that the case $k=0$ is trivial: In the canonical ensemble, $G(\tau,0)$ and $\phi''(\omega,0)$ vanish due to particle conservation.]

In addition to $G(k,\tau)$ we also simulate its first and second derivative, using the relations

$$\frac{d}{d\tau}\langle n_j(\tau)n_{j'}(0)\rangle=\langle[H,n_j(\tau)]_-n_{j'}(0)\rangle = \langle I_j(\tau)n_{j'}(0)\rangle-\langle I_{j-1}(\tau)n_{j'}(0)\rangle \tag{4.16}$$

and

$$\frac{d^2}{d\tau^2}\langle n_j(\tau)n_{j'}(0)\rangle=-\langle[H,n_j(\tau)]_-[H,n_{j'}(0)]_-\rangle = -2\langle I_j(\tau)I_{j'}(0)\rangle+\langle I_{j+1}(\tau)I_{j'}(0)\rangle + \langle I_{j-1}(\tau)I_{j'}(0)\rangle \ , \tag{4.17}$$

where

$$I_j=t(c_j^{\dagger}c_{j+1}-c_{j+1}^{\dagger}c_j) \ . \tag{4.18}$$

We have carried out these simulations for four cases, namely:

(1) A noninteracting, half-filled system with

$$V/t=0, \quad k_BT/t=0.2 \ , \quad N=16, \quad N_F=18 \ .$$

(2) A strongly interacting, half-filled system with

$$V/t=6.0, \quad k_BT/t=0.2, \quad N=16, \quad N_F=8 \ .$$

(3) A strongly interacting, half-filled system with

$$V/t=12.0, \quad k_BT/t=0.2, \quad N=16, \quad N_F=8 \ .$$

(4) A strongly interacting, less than half-filled system with

$$V/t=6.0, \quad k_BT/t=0.2, \quad N=16, \quad N_F=7 \ .$$

The Trotter number in runs (1), (2), and (4) was $L=25$, corresponding to an imaginary-time "slice" $\Delta\tau\equiv\beta/L=0.2/t$.[8] In each run, 2000 fermion configurations were sampled,[8] which took of the order of 10 hours of CPU time per run [total CPU time for all $G(\tau,k)$ and derivatives measured] on a VAX 750, using a standard Fortran program. In run (3) we chose $L=40$ and hence $\Delta\tau=0.125/t$.

The statistical errors ($\Delta G^{(m)}_{\rm MC}$) in our $G(\tau)$ data were of the same order of magnitude at all τ_i, typically 0.5–1.0% of the value of $G^{(m)}(\tau=0)$. The relative error $\Delta G^{(m)}_{\rm MC}/G^{(m)}(\tau_i)$ was therefore quite small near $\tau=0$ and $\tau=\beta$ (0.5–1.0%), but substantially larger (10–100%) at intermediate values of τ ($\tau\sim\beta/2$), since, for the cases considered, $G^{(m)}(\tau)$ becomes very small in this region [typically $G(\tau=\beta/2)/G(\tau=0)\sim10^{-2}$–$10^{-3}$].

B. Noninteracting fermions

In this case, an exact solution can be obtained for the grand canonical problem. For a reasonably sized system,

the grand-canonical and canonical results are essentially equivalent except for the trivial case of zero wave vector. The single-particle energy is

$$\epsilon(p) = -2t\cos p \ . \tag{4.19}$$

For a finite system with periodic boundary conditions, the wave vector p is restricted to the discrete values (4.6) and $\phi''(\omega,k)$ has the form

$$\phi''(\omega,k) = \sum_p A_{k,p}\delta(\epsilon(p+k)-\epsilon(p)-\omega) \ , \tag{4.20}$$

where, in the grand-canonical ensemble,

$$A_{kp} = \pi N^{-1}(1-f_{p+k})f_p \ , \tag{4.21}$$

$$f_p = 1/(1+\exp\{\beta[\epsilon(p)-\mu]\}) \ , \tag{4.22}$$

and for a half-filled system,

$$\mu = 0 \tag{4.23}$$

at all temperatures. Note that in the infinite system limit ($N\to\infty$) the sum over the wave vectors p in (4.20) goes over into an integral. Instead of the densely spaced, discrete δ-function peaks, $\phi''(\omega,k)$ exhibits then a "smeared-out" continuum.

For temperatures that are small compared to the bandwidth, $k_B T \ll 4t$, the system is essentially in the ground state, and the only excitations in (4.20) are particle-hole excitations across the Fermi point, $p_F = \pi/2$. These are sketched schematically in Fig. 3: For small momentum transfer, $k \ll \pi$, we expect a narrow spectrum at small energies $\omega \sim v_F k \equiv 2tk$. As k increases, more and more lines should appear, distributed over an energy range up to the full bandwidth $4t$. In Fig. 4, we show the results for $\phi''(\omega,k)$, obtained from the MC data with the conversion method described in Sec. III. Also shown is the exact result for the grand-canonical case (4.20). (The δ functions are displayed as Lorentzians of finite width [full width at half maximum (FWHM)], $\delta\omega = 0.2t$, and area $A_{k,p}$, given by (4.21).) Notice that the fit to the MC data follows the exact result very systematically: With increasing k, the spectrum becomes broader, and its center moves to larger frequencies.

Note that, in general, due to the noise in the input data, the individual δ functions in $\phi''(\omega,k)$ cannot be resolved by the fit procedure. Let us emphasize, however, that in the infinite system limit, this detailed δ-function structure is not of physical interest. As we increase the system size, an increasing number of more and more densely spaced δ-function peaks appears in the spectrum, each of them carrying less and less weight. Physically relevant then, is only some smeared-out average of $\phi''(\omega,k)$ over a frequency width of the order of one larger than the typical level spacing. The finite width of our rectangular blocks, ΔW, takes this "infinite system smearing," at least crudely, into account. For comparison, the infinite system limit of $\phi''(\omega,k)$ is also displayed in Fig. 4. Note that for wave vectors up to $k = 5\pi/8$, there is good agreement between the fit and the infinite system result. For larger k, the agreement is at best qualitative due to both the finite-size effect and statistical fluctuations.

We have also used the MC data for the noninteracting

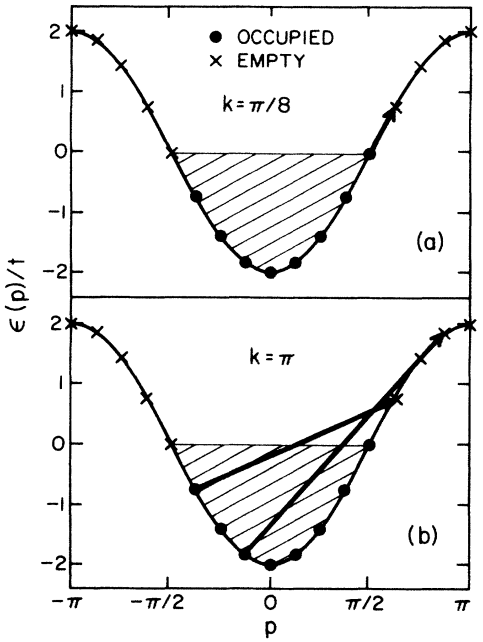

FIG. 3. Particle-hole excitations of a noninteracting 1D fermion system for (a) small and (b) large momentum transfer k.

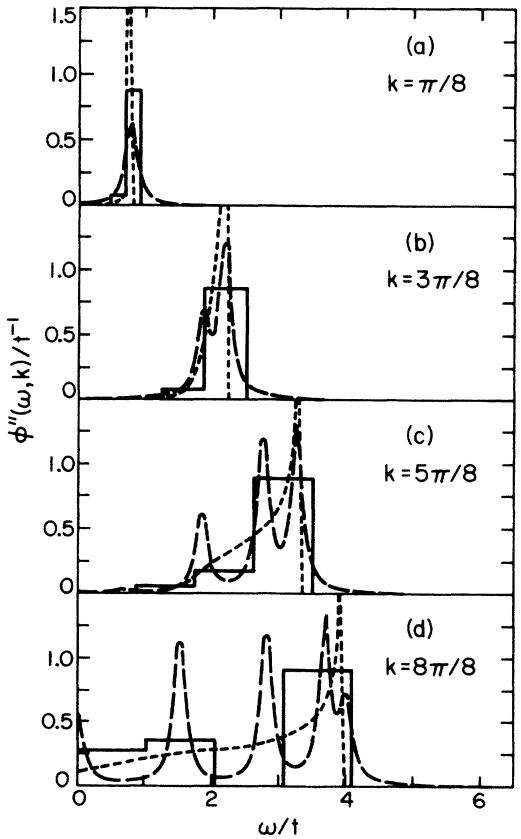

FIG. 4. Spectral function $\phi''(\omega,k)$ of a noninteracting half-filled fermion system with $V=0$, $k_3 T/t = 0.2$ at several wave vectors k; fit result ϕ_F (——); exact result for $N=16$, $N_F=8$ (— — —), exact result for $N\to\infty$ (· · · ·).

system to test the stability of the fit results. Remember that the total width W of the fitted spectra in Fig. 4 was determined by the procedure outlined in Sec. III, i.e., by minimizing the least-squares function, $S_F(W)$, for a trial function $\phi_F(\omega;b_1^2,\ldots,b_4^2)$ with $F=4$ blocks. In Fig. 5(a), we have plotted $S_F(W)$ versus W, obtained for the set of MC data $G^{(m)}(\tau_i,k)$ at wave vector $k=5\pi/8$ with $F=4$ (solid curve) and also for $F=3$ and $F=2$. Focusing on the case $F=4$, we note that $S_4(W)$ exhibits three local minima at $W_4(0)$, $W_4^{(1)}$, and $W_4^{(2)}$, respectively, where $W_4^{(0)}<W_4^{(1)}<W_4^{(2)}$ and $S_4[W_4^{(0)}]<S_4(W_4^{(1)})<S_4(W_4^{(2)})$. The absolute minimum is hence at $W=W_4^{(0)}$. The fitted trial function $\phi_4(\omega;b_1^2,\ldots,b_4^2)$ obtained for this particular value of W [with $b_1,\ldots,b_4$ chosen so as to minimize $S(b_1^2,\ldots,b_4^2)$, Eq. (3.10)] is the result shown in Fig. 4(c) (for $k=5\pi/8$).

To understand the significance of the other two minima, $W_4^{(1)}$ and $W_4^{(2)}$, we have displayed the fitted trial functions $\phi_4(\omega;b_1^2,\ldots,b_4^2)$, obtained for $W=W_4^{(1)}$ and $W=W_4^{(2)}$ in Figs. 5(b) and 5(c), respectively. Clearly, all three results are very similar. They approximate the exact spectral function adequately in the way in which their intensity is distributed on the frequency axis. The difference between them lies in their resolution: As we increase W from $W_4^{(0)}$ to $W_4^{(1)}$, say, the blocks become broader and their center position moves "outward" (to larger frequencies). Obviously, there is a limiting value. W_c, say, somewhere between $W_4^{(0)}$ and $W_4^{(1)}$, such that, for $W>W_c$, the fourth (rightmost) block ($W-\Delta\omega<\omega<W$) falls into a frequency regime where the spectrum has zero intensity. The fit procedure "recognizes" this correctly: It sets the rightmost amplitude $b_4=0$ [as, for example, in Fig. 5(b)] when $W>W_c$ and only allows the first three amplitudes, b_1,b_2,b_3, to vary and, eventually, attain nonzero values. The fit result $\phi_4(\omega;b_1^2,\ldots,b_4^2)$ for a value $W>W_c$ is therefore identical with the fit result $\phi_3(\omega;b_1^2,\ldots,b_3^2)$ that one would obtain by allowing only $F=3$ blocks in the trial function, and, instead of W, a spectral width $W'=3W/4$. This clarifies the role of the second minimum in $S_4(W)$ [at $W_4^{(1)}$]: It corresponds to the best possible fit that can be obtained with $F=3$ blocks. Note that the right edge of the third block in Fig. 5(b) [located at $3W_4^{(1)}/4$] coincides exactly with the position of the local minimum of the least-squares function $S_3(W)$ and, more generally,

$$S_3(3W/4)=S_4(W),\quad W>W_c\ . \tag{4.24}$$

The occurrence of a third minimum of $S_4(W)$ at $W_4^{(2)}$ can be understood analogously. As we increase W from $W_4^{(1)}$ to $W_4^{(2)}$, a second limiting value W_d, say, will be reached, beyond which the two rightmost blocks falls into a spectral region of vanishing intensity and the fit procedure will set $b_3=b_4=0$. The fit result $\phi_4(\omega;b_1^2,\ldots,b_4^2)$ for a spectral width $W>W_d$ is hence identical with the $\phi_2(\omega;b_1^2,b_2^2)$ that would be obtained for a width $W'=2W/4=W/2$. Analogous to (4.24), we have

$$S_2(W/2)=S_4(W),\quad W>W_d\ ; \tag{4.25}$$

the right edge of the second block in Fig. 5(d) [at $W_4^{(2)}/2$] coincides with the minimum of $S_2(W)$.

One further feature to be noted in Fig. 5(a) is the fact that the first (absolute) minimum of $S_F(W)$ becomes shallower when F, the number of blocks, increases. At the same time, the minimal value $S_F[W_F^{(0)}]$ saturates to some final value

$$S_\infty=\lim_{F\to\infty} S_F[W_F^{(0)}]\le S_F[W_F^{(0)}]\ , \tag{4.26}$$

as shown in Fig. 6. To test our method with a larger number of blocks, we have computed $S_F(W)$ for $F=8$. We find that (as for the smaller F, $F=2,3,4$) the exact upper cutoff of the spectrum ($W_x\sim 3.4t$) is clearly visible in $S_F(W)$. As we decrease W to values below W_x, $S_F(W)$ increases steeply, indicating that with $W<W_x$, a good fit to the MC data cannot be obtained. However, the first few local minina, especially the absolute minimum, $W_8^{(0)}$, are hardly visible anymore. Nevertheless, although the absolute minimum of $S_F(W)$ is not very well defined, we

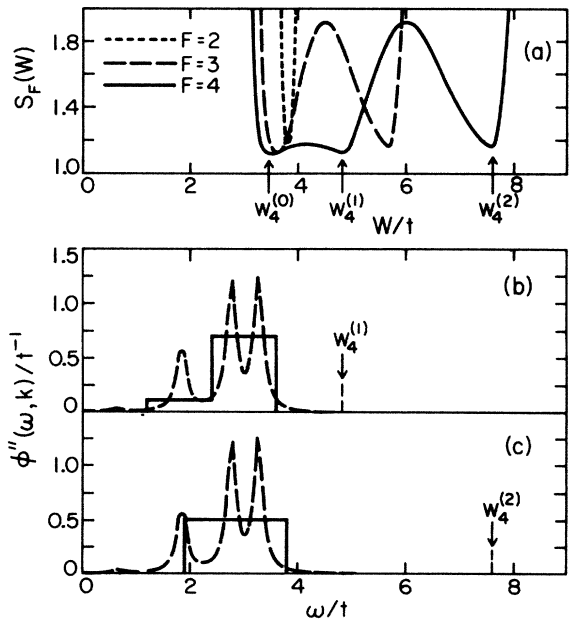

FIG. 5. (a) Minimized sum of squares $S_F(W)$ as a function of the total spectral width W, obtained for the $k=5\pi/8$ MC data of the noninteracting fermion system and $F=2,3,4$; also shown are fit results $\phi_F(F=4)$ for the spectral function, obtained at those values of W where $S_4(W)$ exhibits secondary local minima, (b) $W=W_4^{(1)}$, and (c) $W=W_4^{(2)}$.

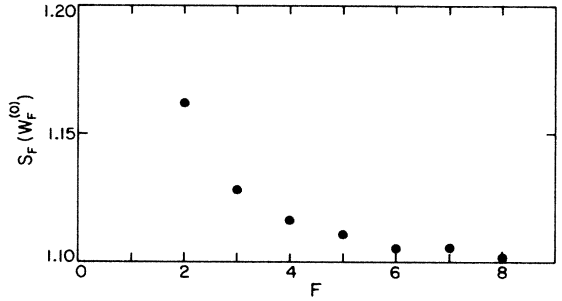

FIG. 6. Absolute minimum, $S_F[W_F^{(0)}]$ versus F for the $k=5\pi/8$ MC data of the noninteracting fermion system.

still get physically reasonable fit results for the spectral function. We have evaluated ϕ_F for several arbitrary values of $W \geq W_8^{(0)}$. Again, we find that as W increases (and hence the blocks broaden and their center positions move outward, the fit procedure assigns the appropriate intensity to those blocks which happen to be at the right frequency. The qualitative features of the fit result are hence quite stable against changes in the parameters W and F.

To demonstrate the importance of the constraint (3.12), requiring ϕ_F to be non-negative, we have displayed in Fig. 7 the fit result (again for the MC data with $k=5\pi/8$). $\phi_4(\omega;a_1,\ldots,a_4)$, obtained by minimizing $S(a_1,\ldots,a_4)$ without the constraint (3.12). In comparison with the previously discussed result, Fig. 4(b) obtained *with* the constraint, it becomes obvious that the constraint improves the result drastically. Without it, a physically meaningful fit result cannot be achieved.

To test the usefulness of measuring MC data for the τ derivatives of $G(\tau,k)$, we have also carried out fits where only $G(\tau,k)$ data, but not $G^{(1)}(\tau,k)$ or $G^{(2)}(\tau,k)$ were included in the sum of squares (3.10). The results for ϕ_F obtained without derivatives are (in the noninteracting case) essentially the same as those shown in Fig. 4. Therefore, we conclude that it is sufficient to measure only the zeroth derivative of $G(\tau,k)$ if a large fraction of the total spectral weight of ϕ'' appears at high frequencies, $\omega \gg k_B T$. Including the independently measured τ derivatives in the fit leads only to marginal improvements of the result. The τ derivatives become very important, however, if ϕ'' contains dominant low-frequency ($\omega \ll k_B T$) components. This occurs, for example, in the strong coupling regime of (4.1), $V \gg t$, where the system exhibits a charge-density wave (CDW) ground state and hence $\phi''(\omega)$ a very strong zero-frequency Bragg peak at $k=\pi$. This will be discussed in the following section.

In concluding this section, let us also briefly discuss the application of other methods that may be used to extract real-frequency spectra from imaginary-time MC data. Clearly, our choice of the trial function ϕ_F, as given by (3.1) and (3.20) is quite arbitrary, and other possibilities should be explored.

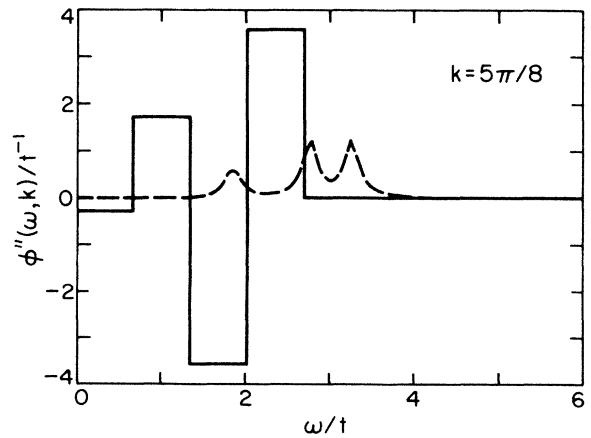

FIG. 7. Fit result for the spectral function $\phi_F(F=4)$ obtained from the $k=5\pi/8$ MC data of the noninteracting fermion system by minimizing (3.10) without the constraint (3.12) fit result (——); exact result for $N=16$, $N_F=8$ (— — —).

As we pointed out above, the spectral function $\phi''(\omega)$ of a finite system is, in general, a superposition of δ functions, corresponding to the discrete excitation energies of the system. Naturally, this suggests that we write ϕ_F as a superposition of terms of the form $a_l\delta(\omega-\omega_l)$ (where $l=1,\ldots,F$, say) and to use both the a_l and the transition energies ω_l as fit parameters to minimize (3.10) [again under the constraint (3.12), i.e., $a_l \geq 0$]. We have carried out such a nonlinear least-squares procedure for the noninteracting Fermion MC data discussed above. At small wave vectors ($k=\pi/8, 2\pi/8$) where the spectra exhibit essentially only one narrow peak [e.g., as in Figs. 4(a) and 4(b)], the fit results we find are in good agreement with the exact ones. However, as we go to larger k and, hence, multiple peak structures (e.g., Figs. 4(c) and 4(d)] the fit fails to resolve the details of this structure. For example, in trying to fit the MC data at $k=\pi$ with a superposition of $F=4$ δ functions (with variable positions $\omega_1,\ldots,\omega_4$ and amplitudes $a_1,\ldots,a_4$), we find that three of these δ functions "collapse" into one single peak (e.g., $\omega_2 \cong \omega_3 \cong \omega_4$), i.e., the fit result ϕ_F exhibits essentially only two-peak structure instead of the four-peak structure that one would expect from the exact $\phi''(\omega,k)$ shown in Fig. 4(d). The difficulty that arises here is that too many fit parameters enter into the problem: The statistical error in the MC data simply does not warrant a sufficiently accurate determination of all the parameters. Clearly, this "inflation" of fit parameters becomes more severe when we increase the system size, and hence the number of δ-function peaks entering into the spectrum. Therefore, based on our experience, we feel that this "δ function" method is not feasible in the case of many-particle systems, since sufficiently accurate MC data would require prohibitively long computation time.

In this connection, we should point out that the δ-function method is, essentially, equivalent to the Padé approximant approach, proposed in Ref. 4. Here, one attempts to carry out an analytical continuation of the imaginary-frequency data ϕ ($z=i\omega_n$), obtained from the corresponding $G(\tau)$ by Fourier transform [Eq. (2.12)]. The two-sided Laplace transform $\phi(z)$ is approximated by a rational (meromorphic) function[4] with finite number of poles on the real axis and $\phi(z) \sim 1/z$, $|z| \to \infty$. Using (2.8), it is easy to see that the corresponding spectrum $\phi''(\omega)$ is just the superposition of δ-function terms $a_l\delta(\omega-\omega_l)$, discussed above.

As a third approach, we have used as a trial function ϕ_F an "educated guess" of its analytical structure: Suppose that, on the basis of certain physical insight (or *prejudice*), such as approximate analytical treatments, we "know," at least roughly, its analytical form, but lack the knowledge of certain parameters that enter into it. We can then use this analytical form as the trial function and adjust the unknown parameters to fit the MC data. We have carried out such an approach, again for the MC data of a noninteracting Fermion system, using as a guess for the analytical form the exact infinite system limit of $\phi''(\omega,k)$, Fig. 4. These functions (for all values of k) can be naturally parametrized by the total intensity, an upper-

and a lower-frequency cutoff, and a certain thermal smearing of the low-frequency cutoff. By adjusting these four parameters to fit the data, reasonable agreement with the exact infinite system results could be obtained. This agreement may seem surprising, at first sight, since the MC data were obtained for a finite system. To understand this, let us note that despite the very different shapes of the finite and the infinite system spectral functions, $\phi''(\omega,k)$, displayed in Fig. 4, the difference in the corresponding imaginary-time functions $G^{(m)}(\tau,k')$ is typically of the order of (or less than) 1% of $G^{(m)}(0,k)$ and hence of the same order as the statistical error of the MC data. In conclusion, we can say that the method of "analytical guesses" may be used complementary to the "histogram" method. Assuming such an analytical guess may allow measuring more easily the dependence of certain spectral features (such as gaps, linewidths, etc.) on model parameters, temperature, etc. On the other hand, the histogram approach has the advantage that it is "unprejudiced" in that no particular analytical shape has to be assumed.

C. Strongly interacting fermions

If $V>2t$, the half-filled infinite system (4.1) exhibits a charge-density-wave (CDW) ground state.[6,7] For $t=0$, the Hamiltonian becomes site diagonal. The ground state is then a configuration of alternatingly occupied and empty sites, and, as shown in Fig. 8(a), there are two equivalent, energetically degenerate ground-state configurations, A and B, say. The lowest excited state consists[6,9,10] of a pair of domain walls (soliton-antisoliton pair) separating segments of A- and B-type ground-state configurations, as shown in Fig. 8(b). The single-pair state is highly (approximately N^2-fold) degenerate and has an excitation energy V (relative to the ground state). Analogously, n-pair states with energies nV ($n=1,2,3,\ldots$) can be created, as shown in Fig. 8(c) for $n=2$.

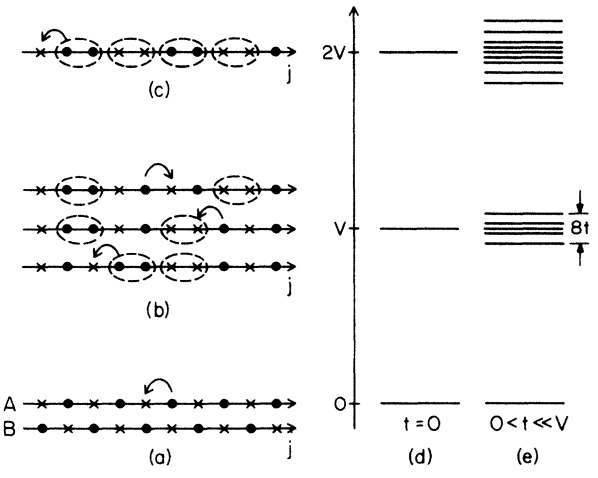

FIG. 8. (a) Ground state, (b) soliton-pair, and (c) two soliton-pair configurations of the strongly coupled half-filled fermion system ($V/t\to\infty$); ●, occupied; χ, empty lattice sites. In (d) and (e) the excitation energies and, respectively, the broadening due to intersite transfer, are indicated.

As we "turn on" a small, but finite intersite transfer, $0<t\ll V$, the degeneracies are lifted and the n-pair states are broadened into bands of a finite width of the order of t.[9] As long as this bandwidth ($\sim t$) is small compared to the spacing V between adjacent bands, we may (in lowest order) neglect the mixing between states from different bands so that the soliton-pair number, n, remains a good quantum number. To be specific, let us consider the eigenstates of the lowest ($n=1$) soliton-pair band. In an infinite system, they are scattering states characterized by the asymptotic wave vectors, p and p', of the soliton pair involved and by an energy (relative to the ground state)

$$E(p,p')=V+\epsilon_s(p)+\epsilon_s(p')\ , \tag{4.27}$$

where $\epsilon_s(p)$ is the band energy of a single (anti) soliton with a wave vector p and spatially "far" away from its counterpart. Neglecting the admixture from other bands (i.e., renormalization due to virtual pair excitations), $\epsilon_s(p)$ is given by[9]

$$\epsilon_s(p)=-2t\cos(2p)\ . \tag{4.28}$$

Note that, different from the free-particle band (4.19), a factor of two occurs in the argument of the cosine of (4.28), reflecting the fact that the soliton is located in the CDW superlattice with a lattice constant twice that of the underlying chain: As indicated in Fig. 8(b), the soliton is transferred by two lattice sites, due to the transfer of a fermion by one site. Combining (4.28) and (4.27), one finds that the excitation energy needed to create a soliton-antisoliton pair with total momentum $k=p+p'$ from the ground state is limited by energy and momentum conservation, namely

$$\omega_-(k)\le E(p,k-p)\le\omega_+(k) \tag{4.29}$$

where

$$\omega_-(k)=V-|\,4t\cos(2k)\,|\ , \tag{4.30}$$

$$\omega_+(k)=V+|\,4t\cos(2k)\,|\ . \tag{4.31}$$

At low temperatures, $k_BT\ll V$, the spectral function $\phi''(\omega,k)$ should therefore exhibit an absorption peak around $\omega\sim V$, spread out over a width

$$\Gamma(k)\equiv\omega_+(k)-\omega_-(k)=|\,8t\cos(2k)\,|\ . \tag{4.32}$$

Note that Γ is maximal ($\Gamma\sim 8t$) both for small ($k\to 0$) and large ($k\to\pi$) wave vectors and exhibits a minimum, at $k=\pi/2$: In the lowest-order approximation (neglecting interband mixing), the soliton-pair states with total wave vector $k=\pi/2$ do actually remain degenerate and $\Gamma=0$. However, taking the corrections due to the admixture from higher bands into account, these states will also be broadened (over a width of the order $\Gamma\sim t^2/V$). A detailed lowest-order calculation of the contribution, $\phi_1''(\omega,k)$, to the spectral function, arising from the single pair creation, has been carried out by Ishimura and Shiba.[10] They find, in agreement with our qualitative kinematical arguments, that for $k_BT=0$ and $N\to\infty$

$$\phi_1''(\omega,k)=-8\frac{t^2}{V^2}\frac{\sin^2(k/2)}{\Gamma(k)/2}\left[1-\left[\frac{\omega-V}{\Gamma(k)/2}\right]^2\right]^{1/2} \tag{4.33}$$

for $\omega_-(k)\leq\omega\leq\omega_+(k)$ and vanishing otherwise. Note that the total intensity of $\phi_1''(\omega,k)$ is strongly k dependent:

$$I_1(k)\equiv\int d\omega\phi_1''(k,\omega)\propto\sin^2k/2\ . \tag{4.34}$$

In addition, we expect to see similar absorption peaks around $\omega\sim2V$, $\omega\sim3V,\ldots,$ corresponding to the creation of two pairs, three pairs, and so on. However, the total intensity of these contributions should be smaller than that of $\phi_1''(\omega,k)$ by factors of the order (t/V), $(t/V)^2$, etc.

Finally, let us point out that the spectral function will exhibit a "Bragg" peak at $k=\pi$ and $\omega=0$, due to the "long"-range order of the CDW ground state: Although the 1D system cannot exhibit true long-range order for $k_BT>0$, the correlation length ξ of $\langle n_jn_{j+l}\rangle\sim\exp(-l/\xi)$ is typically of the order $\xi\sim\exp(V/k_BT)$ for t, $k_BT\ll V$ and hence, at our parameter values, large compared to the system size N. To allow for such a Bragg peak in the spectral function, we have included in the trial function (3.1) a term

$$a_0\phi_0(\omega)\equiv a_0\delta(\omega)\ , \tag{4.35}$$

with adjustable amplitude a_0, in addition to the rectangular blocks $\phi_l(\omega)$, (3.20).

In Figs. 9 and 10, we display our fit result, obtained from MC data for $V=6t$ and $V=12t$, respectively, at $k_BT=0.2t$ on a half-filled 16-site chain. Also shown is the strong-coupling result (4.33).[10] The MC result shows the expected behavior: an absorption peak around $\omega\sim V$ with an intensity that increases with k. For certain k, an additional peak around $\omega\sim2V$ is also visible. In contrast to the free fermion spectrum [Fig. 4(a)], the peak position $(\omega\sim V)$ is roughly constant for all k. Also note the difference in frequency scale and intensity between Figs. 4, 9, and 10. The peak width of the MC result in Figs. 9 and 10 is generally smaller than that predicted by (4.33). This should not be too surprising, since, for our parameter values, the width Γ, Eq. (4.32), is typically of the same order as the interband spacing V: The lowest-order strong-coupling result is therefore, at best, qualitatively correct. For a quantitative description, the interband mixing would have to be taken into account.

Finally, let us turn to the elastic $(\omega=0)$ contribution (4.35). We have allowed such a term in the trial function ϕ_F at all wave vectors. However, for $k\neq\pi$, the fit procedure results in $a_0=0$, indicating that, as expected, no elastic scattering with momentum transfer $k\neq\pi$ occurs. For $k=\pi$, on the other hand, the elastic intensity a_0 under the δ function (represented by a rectangular block

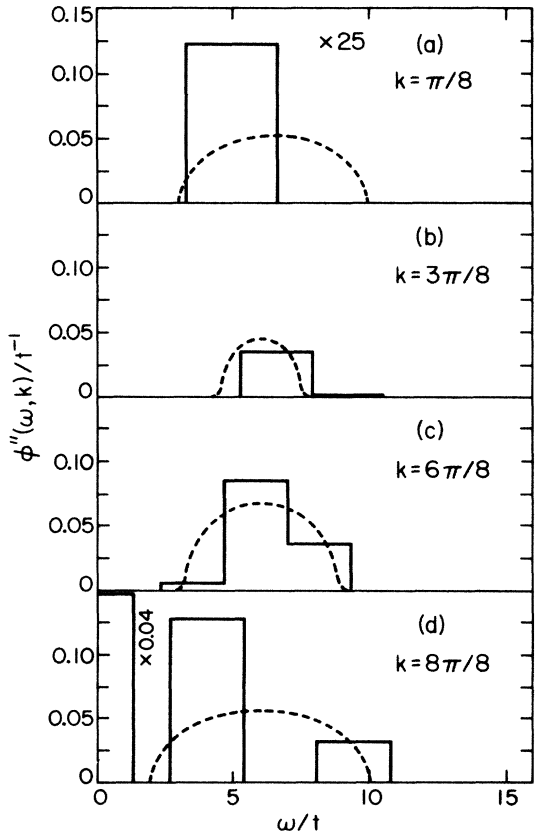

FIG. 9. Spectral function $\phi''(\omega,k)$ of a strongly coupled half-filled fermion system with $V/t=6.0$, $k_BT/t=0.2$ at several wave vectors k; fit result ϕ_F (——), analytical strong-coupling result (Ref. 10) for $N\to\infty$, $k_BT=0$ (· · · ·).

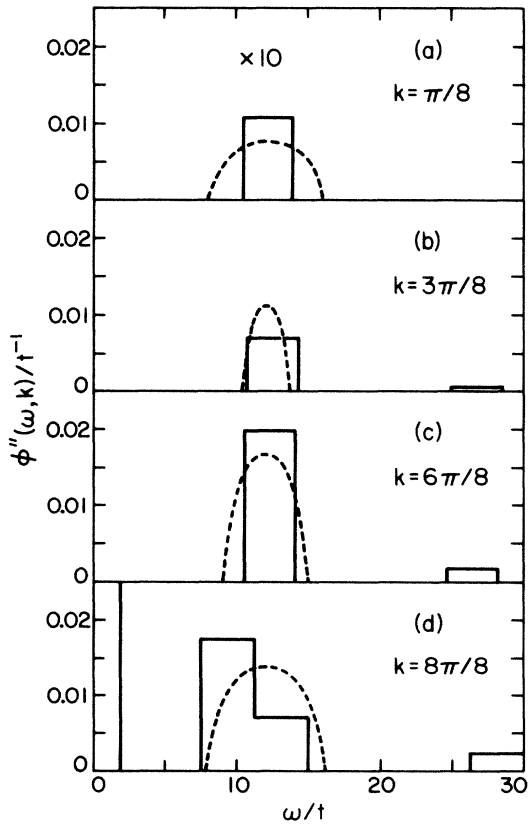

FIG. 10. Spectral function $\phi''(\omega,k)$ of a strongly coupled half-filled fermion system with $V/t=12.0$, $k_BT/t=0.2$ at several wave vectors k; fit result ϕ_F (——), analytical strong-coupling result (Ref. 10) for $N\to\infty$, $k_BT=0$ (· · · ·).

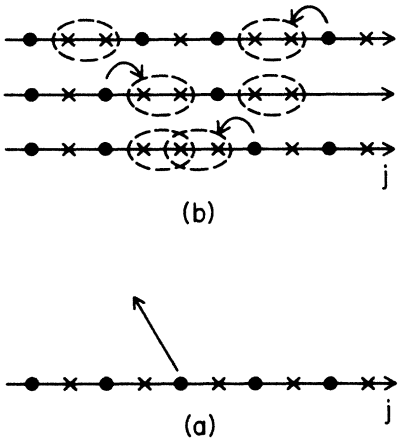

FIG. 11. Ground-state configurations of a strongly coupled fermion system; (a) half-filled; (b) less than half-filled (after removing one fermion from the half-filled system).

of width $\Delta W/2$ centered at $\omega=0$) is about 20 times larger than the total inelastic intensity of $\phi''(\omega,\pi)$. Nevertheless, the inelastic part can still be measured, since, in the first and second derivative of $G(\tau,k)$, the elastic part is filtered out. In this case, it is hence crucial to take the τ derivative of $G(\tau,k)$ into account.

If we remove one fermion from the CDW ground state of the half-filled system, the new system will exhibit a soliton pair already in its ground state (see Fig. 11). Its low-temperature excitation spectrum should hence differ significantly from that of the half-filled case. Namely, $\phi''(\omega,k)$ should exhibit structure at low frequencies due to the inelastic scattering from a single soliton as well as scattering off the soliton pair.[9,10]

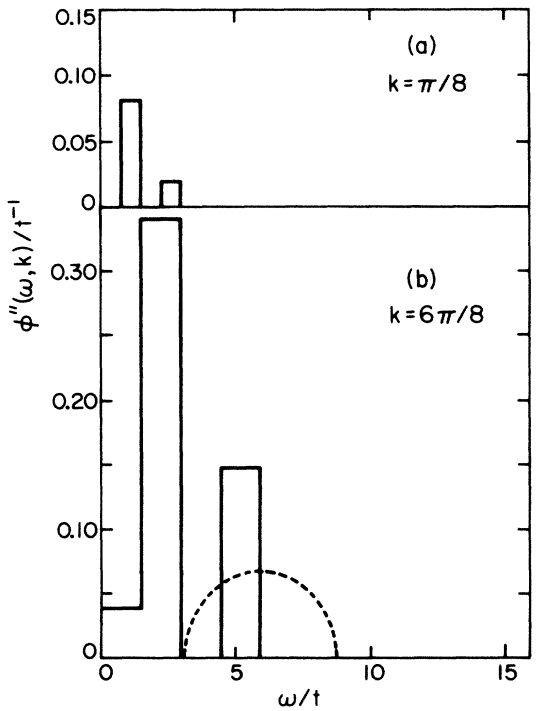

FIG. 12. Spectral function $\phi''(\omega,k)$ of a strongly coupled less-than-half-filled fermion system with $V/t=6.0$, $k_BT/t=0.2$, $N=16$, and $N_F=7$, at several wave vectors; k; fit result ϕ_F ($F=9$) (——), analytical strong-coupling result (Ref. 10) for the exactly half-filled system and $N\to\infty$, $k_BT=0$ (. . . .).

In Fig. 12 we show the fit result obtained from MC data for $V=6t$ and $k_BT=0.2t$ on a (less than half-filled) 16-site chain with 7 fermions. It indeed differs drastically from the half-filled case shown in Fig. 9. Although an analysis in terms of the strong-coupling soliton energy band, Eq. (4.28), does not seem feasible (again, due to the substantial interband mixing for the parameter values chosen), the shift of the spectral weight to low frequencies $\omega<V$ is clearly visible.

V. CONCLUSION

We have proposed a method to extract information about the real-frequency correlation functions $S(\omega)$, $\chi''(\omega)$, Eqs. (2.3)–(2.6), from the imaginary-time Green's functions $G(\tau)$, Eq. (2.1), that can be simulated using quantum Monte Carlo techniques. The starting point of our procedure is an integral equation (2.13), relating the real-frequency correlation function $\phi''(\omega)$ to the imaginary-time Green's function. The difficulty in solving this integral equation (to obtain ϕ'') arises from the fact that $G(\tau)$ is fairly insensitive to the detailed structure of $\phi''(\omega)$. Hence, even small statistical errors in the input data, $G(\tau)$, can lead to large errors in the solution $\phi''(\omega)$.

To overcome this difficulty, we propose to measure not only $G(\tau)$ but also, independently, its derivatives $G^{(m)}(\tau)$ [Eq. (3.9)] which contain the same $\phi''(\omega)$, weighted, however, with additional factors ω^m under the integral (3.8). More importantly, we restrict ourselves to self-correlation functions for which $\phi''(\omega)\geq 0$ [Eq. (2.14)]. From the MC data, we obtain $\phi''(\omega)$ by a least-squares-fit procedure: We insert into (3.8) an appropriate trial function $\phi_F(\omega;a_1,\ldots,a_F)$ and vary the fit parameters, $a_1,\ldots,a_F$, such as to minimize the sum of the squared deviations between the MC data for $G^{(m)}(\tau)$ and the corresponding "fitted curve" (3.8). This minimization is carried out under the constraint that $\phi_F(\omega;a_1,\ldots,a_F)\geq 0$ at all ω, thereby taking into account the positivity of $\phi''(\omega)$. We have demonstrated (Fig. 7) that this constraint is essential in stabilizing the fit result against large, unphysical fluctuations. It is worth mentioning at this point that any mixed correlation function $[\phi''_{AB}(\omega), B\neq A^+]$ can be written as a superposition of (at most) three self-correlation functions. Using our conversion method, it is therefore, at least in principle, possible to obtain mixed correlation functions as well (if the corresponding three self-correlation functions can be simulated).

To test our method, we have applied it to a simple 1D model of spinless fermions (4.1): Using the "world-line" MC algorithm,[8] we have simulated the (imaginary-time) density correlation function, $G(\tau,k)$ (4.4) and, independently, its first and second τ derivative for all relevant wave vectors k of the (*finite*) system.

For the case of noninteracting fermions, we have shown that the fit result is in qualitative agreement with the exact spectral function $\phi''(\omega,k)$ (Fig. 4). We have demon-

strated that the fit result is (at least qualitatively) stable against variations of certain "arbitrary" parameters (F, W) that enter into the trial function ϕ_F (Fig. 5), provided the positivity constraint (3.12) is taken into account (Fig. 7).

Furthermore, we have compared our procedure to other possible methods of converting imaginary-time MC data into real-frequency spectral functions, namely analytical continuation via Padé approximants[4] and analytical guesses. Based on our experience, we conclude that the recently proposed Padé approach[4] and its equivalents are not feasible for many-particle systems, given the limited statistical accuracy that MC methods typically allow one to achieve. On the other hand, an educated guess of the analytical form of the spectrum with only a few adjustable parameters may well provide additional insight into the problem.

In this connection it is worthwhile to discuss the possibility of a direct simulation of real-time correlation functions that has recently been proposed for simple model systems.[3] Attempts to implement such an approach for many particle systems have not been successful.[11] Due to certain strongly fluctuating phase factors that enter into the MC summation, the "measurement" of the real-time quantities converges very slowly and hence requires prohibitively long simulation times.[11] Very similar problems arise in direct simulations of the real-frequency spectra which, again, have so far only been successful for very simple (one degree-of-freedom) systems.[2]

We have also treated the case of strongly interacting half-filled systems, exhibiting a CDW ground state and soliton-antisoliton pair excitations (Fig. 8).[6,7,9,10] The absorption peaks corresponding to the creation of one and two pairs, respectively, are clearly visible in the fit result for $\phi''(k,\omega)$ (Figs. 9 and 10). They occur in the expected frequency regions $\omega \sim V$ and $\omega \sim 2V$, and their intensity shows roughly the expected wave-vector dependence.

Finally, we have considered the case of a strongly interacting, less-than-half-filled system, containing one soliton pair ("immersed" in the CDW ground state). Again, the expected behavior[9,10] [namely, the existence of low-frequency excitations due to scattering from the soliton (pair)] is realized in the fit result.

Considering the lack of detailed quantitative agreement between our fit results and the exact solution (e.g., for the noninteracting Fermion case), the question of how to improve these results arises. First of all, one should, of course, try to enhance the resolution of the trial function ϕ_F, by increasing the number of blocks F. Using the MC data underlying Fig. 4 we have carried out such fits with block numbers up to $F=8$. The results for the intensity distribution $\phi_F(\omega)$, are very similar to those shown in Fig. 4 (where $F=4$). However, they do not show substantial improvement in their quantitative agreement with the exact results. Also, the minimized value of the sum of the squared deviations Eq. (3.10) decreases only by a few more percent as we increase the number of blocks from $F=4$ to $F=8$. This indicates that most of the information about $\phi''(\omega)$ contained in the given set of $G(\tau)$ data has been exhausted by the "$F=4$" fit. Nevertheless, it is encouraging to see that the results with different F values are at least stable, i.e., qualitatively in agreement with each other.

We therefore believe that better results for the spectral function $\phi''(\omega)$ will necessarily require an improved statistical accuracy of the input data $G(\tau)$, in addition to an enhanced resolution of the trial function ϕ_F. For example, we have applied our method to $G(\tau)$ data that were obtained by randomly superimposing a certain noise level on the exact $G(\tau)$ values that are readily available for the noninteracting system. Indeed, we find a significant improvement of the fit results if the noise level $\Delta G_{\mathrm{MC}}^{(m)}$ is reduced by factors of 3—10 from that present in our MC data. It is not unrealistic to assume that such an improved accuracy of the MC data can be achieved within reasonable time by use of faster computation facilities. Nevertheless, we feel that even with the given level of accuracy, our method can provide useful insights.

In conclusion, we have demonstrated that our method allows one to extract qualitative features of real-frequency spectra of many particle systems from imaginary-time data, simulated within reasonable amounts of computation time.

ACKNOWLEDGMENTS

We would like to thank Dr. M. Imada for many helpful discussions. This material is based upon work supported by the National Science Foundation under Grant No. DMR83-20481. We gratefully acknowledge E. I. du Pont de Nemours and Company and the Xerox Corporation for their support.

[1] *Applications of the Monte Carlo Method in Statistical Physics*, edited by K. Binder (Springer-Verlag, Berlin, 1984); *Monte Carlo Methods in Quantum Problems*, NATO Advanced Study Institute Series B, edited by M. H. Kalos (Reidel, Dordrecht, 1984).

[2] J. E. Hirsch and J. R. Schrieffer, Phys. Rev. B **28**, 5353 (1983).

[3] E. C. Behrman, G. A. Jongeward, and P. G. Wolynes, J. Chem. Phys. **79**, 6277 (1983).

[4] D. Thirumvalai and B. Berne, J. Chem. Phys. **79**, 5029 (1983).

[5] H.-B. Schüttler and D. J. Scalapino (unpublished).

[6] J. Hubbard, Phys. Rev. B **17**, 494 (1978), and references cited therein.

[7] A. Luther and I. Peschel, Phys. Rev. B **12**, 3908 (1975).

[8] J. E. Hirsch, R. L. Sugar, D. J. Scalapino, and R. Blankenbecler, Phys. Rev. Lett. **47**, 1628 (1981); Phys. Rev. B **26**, 5033 (1982).

[9] J. Villain, Physica **79B**, 1 (1975).

[10] N. Ishimura and H. Shiba, Prog. Theor. Phys. **63**, 743 (1980).

[11] R. L. Sugar and D. J. Scalapino (unpublished).